Suboxide interface in disproportionating *a*-SiO studied by x-ray Raman scattering

A. Sakko,[1,*] C. Sternemann,[2] Ch. J. Sahle,[2] H. Sternemann,[2] O. M. Feroughi,[2] H. Conrad,[2,3] F. Djurabekova,[1] A. Hohl,[4] G. T. Seidler,[5] M. Tolan,[2] and K. Hämäläinen[1]

[1]*Department of Physics, P. O. Box 64, FI-00014, University of Helsinki, Finland*

[2]*Fakultät Physik/DELTA, TU Dortmund, D-44221 Dortmund, Germany*

[3]*Deutsches Elektronen-Synchrotron (DESY), D-22603 Hamburg, Germany*

[4]*Institute for Materials Science, Darmstadt University of Technology, 64287 Darmstadt, Germany*

[5]*Department of Physics, University of Washington, Seattle, Washington 98195, USA*

(Received 16 February 2010; revised manuscript received 30 April 2010; published 21 May 2010)

The microscopic structure of disproportionating amorphous silicon monoxide is studied by inelastic x-ray scattering at the silicon $L_{\mathrm{II,III}}$ edge. This material arranges into nanocrystalline regions of Si embedded in amorphous SiO_2 at proper annealing temperatures and in this work we demonstrate how the contribution of the suboxide interfaces between these regions can be extracted from the experimental data. The resulting near-edge spectra are analyzed in detail using a computational framework that combines molecular-dynamics simulations and density-functional theory calculations. The results indicate that the amount of silicon atoms with oxidation states between +1 and +3 is significant and depends strongly on the annealing temperature. Furthermore, the presented *s*, *p*, and *d*-type local densities of states (ℓDOS) demonstrate that the most significant differences are found in the *p*-type ℓDOS.

DOI: 10.1103/PhysRevB.81.205317 PACS number(s): 68.35.Ct, 78.67.Bf, 78.70.Ck

I. INTRODUCTION

Silicon oxides are important materials for present day semiconductor technology and for various potential microelectronic and optoelectronic applications.[1–3] Amorphous silicon monoxide (a-SiO) is of particular interest because its black coal-like modification shows phase separation, i.e., disproportionation to nanocrystalline regions of Si embedded in a-SiO_2 under annealing.[4] It is well acknowledged that embedding of crystalline silicon nanoclusters into silicon dioxide can significantly improve its luminescence properties.[5,6] Unlike bulk silicon with an indirect band gap, Si nanoclusters embedded in SiO_2 show intense visible photoluminescence with wavelengths depending on the size of the nanoclusters.[7] The origin of the phenomenon is intensively debated and various explanations have been proposed.[8–10] In any case the important role of the Si/SiO_2 interface is acknowledged and its structural characterization is of particular importance.

According to the interface clusters mixture (ICM) model, the native (i.e., not annealed) a-SiO consists of amorphous regions of Si and SiO_2 that have diameters of less than 2 nm and where a significant proportion of atoms are located in the interfaces of these regions.[4] The silicon atoms within these interfaces can have a variable number of oxidation states and they are thus called suboxides. Under annealing at elevated temperatures the Si and SiO_2 clusters grow along with interface obliteration and eventually Si nanocrystals form. This structural model is supported by several experimental observations[4,11,12,23] but the knowledge of the detailed structure especially at the interfaces remains ambiguous.

In this work we apply near-edge spectroscopy to study the atomic structure of the internal suboxide interfaces in disproportionating a-SiO. Near-edge spectroscopies, such as x-ray absorption spectroscopy (XAS) and electron energy-loss spectroscopy (EELS) as well as x-ray Raman scattering (XRS), are important probes of the local electronic structure of a wide range of materials.[13] XRS, i.e., inelastic x-ray scattering from inner-shell electronic excitations, in particular, is well suited for studying the electronic excitations of disordered materials due to its bulk sensitivity, applicability under extreme experimental conditions, and the unique information provided by the momentum-transfer dependency.[14] Our approach is based on separating the XRS spectrum into contributions from excitations at nanocrystalline Si regions, at amorphous SiO_2 regions, and at their interfaces. We employ molecular-dynamics (MD) simulations and density-functional theory (DFT) calculations to analyze the interface contribution in detail. The annealing temperature dependency of the disproportionation shows significant structural changes at around 900 °C and a high amount of suboxides in the samples is found. Furthermore, the presented framework provides a method to calculate XRS spectra from MD simulations that can be directly compared with experiments and therefore it can be used to verify the theory by experiment.

II. X-RAY RAMAN SCATTERING

In an inelastic x-ray scattering process a photon scatters from the sample causing an elementary excitation in the material. Within the first-order Born approximation the experimental spectrum is proportional to the dynamic structure factor $S(\mathbf{q},\omega)$, where $\mathbf{q}$ and ω are the momentum and the energy transferred to the sample, respectively (we use atomic units in this work, i.e., $m_e=\hbar=e=1$, except for the numerical values). In an XRS process an inner-shell electron is excited from the core state to one of the unoccupied electronic states. The cross section (and therefore the dynamic structure factor) carries information on the transition rates between the core and unoccupied states. The highly symmetric and localized nature of the inner-shell state enables the interpretation of the spectrum in terms of the symmetry properties of the

unoccupied states in the immediate vicinity of the excited atomic site.[15] One can also obtain detailed structural information on the sample using computational methods that allow an accurate interpretation of the near-edge spectrum. These properties have made XRS, and near-edge spectroscopies in general, very powerful tools for the study of numerous problems in materials science.

The similarity of XRS and XAS is often acknowledged: at low scattering angles both XRS and XAS probe dipole transitions and provide similar information on the sample. At high scattering angles, that is, high-momentum transfers, XRS probes also nondipole transitions and a more complete picture of the electronic structure can be obtained. Because the XRS experiments are carried out with hard x-rays (the incoming energy is typically around 10 keV), the method is insensitive to surface effects and no vacuum is required in the experiments which also makes the measurements at extreme conditions feasible.[16] Even though the low scattering cross section means that the experimental work has to be carried out at synchrotron-radiation facilities, XRS has become a powerful tool for numerous studies where experiments using other techniques would be problematic.[17–22] Concerning this work, the relatively low energy ($\sim$100 eV) of the Si $L_{\mathrm{II,III}}$ edge would make its measurement using soft x-ray absorption surface sensitive which can obscure the information on bulk properties of the system.

A. Experiments

The details of the sample preparation and the experimental work are given in another publication[23] and therefore only a short review is presented here. The samples were prepared by evaporation of a mixture of Si and SiO_2 at 1400 °C and subsequent condensation at about 600 °C. The resulting native a-SiO samples were then annealed at temperatures T_a between 725 and 1200 °C, grounded to powder and finally pressed into pellets. The XRS experiments were carried out at beamline XOR/PNC 20-ID of the Advanced Photon Source using the LERIX spectrometer[24] with an energy resolution of 0.6 eV. The incident-beam energy was 9.89 keV and a set of spectra were measured with momentum transfers between 2.4 and 10.1 Å^{-1} (series A). In an earlier experiment[25] we measured spectra for momentum transfer $q=10.1$ Å^{-1} for native and annealed SiO with an energy resolution of 1.4 eV (series B). Here, also reference spectra of crystalline Si and SiO_2 were taken. The background subtraction was carried out using the framework described in Ref. 25 and the results of series A are shown in Fig. 1.

The evident T_a dependency is due to the structural changes that take place in the sample during annealing, i.e., the clusters grow by coalescence with concurrent obliteration of suboxide interfaces. The interpretation of the annealing temperature dependency is discussed in detail in Ref. 23. The work here focuses on the interface contribution to the spectrum.

The total experimental spectrum of a fully disproportionated SiO is similar to a sum of the Si and SiO_2 spectra. The small differences observed for the native and annealed samples (with $T_a<1200$ °C) reveal that part of the silicon

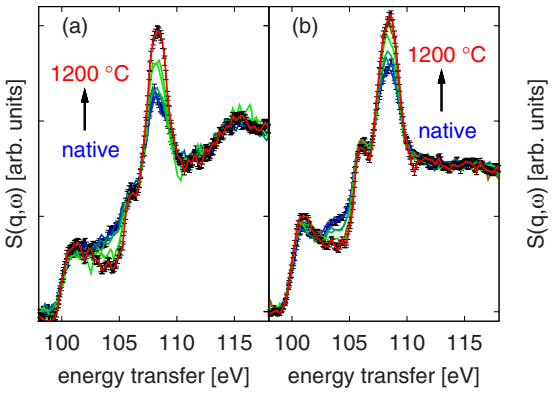

FIG. 1. (Color online) The experimentally measured dynamic structure factors for the different samples at (a) $q=2.4$ Å^{-1} and (b) $q=9.85$ Å^{-1}. The changes between 101 and 110 eV are due to the decreasing suboxide content with the annealing temperature. The high-momentum-transfer spectra were published originally in Ref. 23.

atoms are in a suboxide state. This is in line with the ICM model, as was pointed out in Ref. 11. The suboxidic silicon atoms lie at the interfaces and have oxidation states between +1 and +3. Since XRS is a local probe, the admixture of different phases results in proportional admixture of spectra so that the experimentally measured dynamic structure factor can then be written as

$$S_{\mathrm{exp}}(\mathbf{q},\omega) = (1-a) \times S_{\mathrm{Si+SiO_2}}(\mathbf{q},\omega) + a \times S_{\mathrm{SiO_x}}(\mathbf{q},\omega), \tag{1}$$

where a is the proportion of the suboxidic Si atoms in the sample, $S_{\mathrm{SiO_x}}(\mathbf{q},\omega)$ is the spectrum of the suboxides, and $S_{\mathrm{Si+SiO_2}}(\mathbf{q},\omega)$ is the sum of the spectra of bulk Si and bulk SiO_2, normalized to the same value.[26] Our approach bases on the assumption that the amount of silicon atoms at Si and SiO_2 regions is equal, which implies that the average oxidation state in the suboxide regions is +2. If this would not hold the Eq. (1) would need to be generalized. We discuss this case at Sec. III. Because the interface contribution becomes negligible at high annealing temperatures when the nanocrystalline regions grow larger, the $S_{\mathrm{Si+SiO_2}}(\mathbf{q},\omega)$ can be approximated by the spectrum of the sample annealed at $T_a=1200$ °C.[23]

B. Calculations

The most comprehensive interpretation of the experimental near-edge spectrum is typically obtained by a comparison with calculated spectrum that provides a detailed picture of the electronic structure behind the observed spectral features. Various computational methods for simulating the momentum-transfer-dependent XRS spectra have been developed during the last few years.[27–31]

In order to calculate the dynamic structure factor a structural model for the sample material, i.e., coordinates of the atoms, is needed. The simplest model for the silicon suboxides is the five-atom tetrahedra $SiSi_xO_{4-x}$, where $1\leq x\leq 3$.[4] This model lacks the effect of the other coordination shells

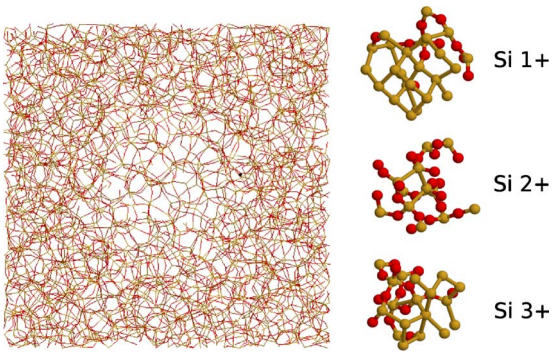

FIG. 2. (Color online) The structure of the internal interfaces was modeled by molecular-dynamics simulations (Ref. 36). From the simulation snapshots (on the left) a set of small Si-centered clusters (on the right) were extracted and then used for density-functional theory calculations.

and in this work we use MD simulations to generate more realistic structures, see Fig. 2.

1. Molecular-dynamics simulations

MD is a powerful tool for generating atomic configurations that can explain many macroscopic properties of materials in terms of their atomic scale structure. However, the simulation of phase transitions can be a very challenging task when the relevant length and time scales are large.[32,33] Hence, in the present work the MD simulation for a system consisting of a silicon nanocrystal (with the diameter of 2.4 nm) embedded in amorphous silicon dioxide was carried out to model the interface between the Si nanocrystal and a-SiO_2. Such an atomistic model can serve as a good approximation to the real suboxide interfaces in the disproportionating a-SiO. The approach is justified by the sensitivity of XRS to the local electronic structure in the vicinity of the excited atomic site. The approximation is that the local atomic structure (e.g., bond lengths and angles) around Si atoms is very similar in the two systems, despite the different long-range order. For the calculations of XRS spectra we extract small model clusters (~35 atoms) around the Si atoms in the interface. This gives a realistic compromise between the simple tetrahedron model and the actual disproportionating a-SiO.

The MD simulations were carried out employing classical interatomic potentials[34,35] that are able to describe bonding of both the ideal structures and the coordination defects. A detailed description of the simulation is given in Ref. 36. The small clusters, centered around randomly selected Si atoms, were extracted from MD snapshots by including the atoms whose distance from the central site is less than 5.0 Å.[37] The clusters were classified according to the oxidation state of the central Si atom, i.e., the number of oxygens that are bonded to it. In the bulk regions of Si and SiO_2 these numbers are 0 and 4, respectively, but in the interfaces the oxidation state varies between 0 and 4. Also defects, i.e., atoms that do not have exactly four neighbors, can appear. MD simulation indeed gives higher defect concentration than expected[4] for a-SiO.

2. Calculations of XRS spectra

The near-edge spectrum for each small model cluster was calculated using the computational method presented for XAS in Refs. 38 and 39 and its extension to XRS.[31] Within the quasiparticle approximation, the dynamic structure factor can be expressed in the form

$$S(\mathbf{q},\omega) = \sum_{i}^{N_{occ}} \sum_{f}^{N_{unocc}} |\langle f|e^{-i\mathbf{q}\cdot\mathbf{r}}|i\rangle|^2 \delta(\omega + \omega_i - \omega_f), \quad (2)$$

where the sums over i and f include all the occupied and the unoccupied electronic states, respectively, and ω_i and ω_f are their energies.[14] The one-electron states are calculated by DFT within transition potential approximation[40] and are expressed using localized Gaussian basis functions. In our calculations the exchange and correlation was approximated by a generalized gradient functional.[41,42] Triple zeta plus valence polarization basis sets were used except for the excited atom site, for which III-IGLO and a set of delocalized diffuse basis functions were used. To ensure the localization of the inner-shell orbital, model core potentials were used for all nonexcited silicon sites.[43,44]

The calculation neglects the spin-orbit coupling that causes a 0.6 eV splitting of the Si $2p$ level and therefore some additional smearing of the spectrum. Because the core hole can occupy any of the three $2p$ orbitals, individual calculations were carried out for each of them. When setting the half occupancy to one of these orbitals, their eigenvalue ordering changes and therefore the three calculations are not independent. However, due to the similar nature (p-type symmetry and the degree of localization) of the three orbitals the three directionally averaged spectra are very similar (they probe the same unoccupied states of the same symmetry at the same region of space). As an example, the method has been shown to give good results for the q-dependent Si $L_{\mathrm{II,III}}$ edge XRS spectrum of SiO_2.[25]

Another challenge for the calculations is the possible excitonic nature of the main transition in the suboxides. The Si $L_{\mathrm{II,III}}$ XRS near-edge spectrum of bulk silicon[45] is dominated by an exciton peak that poses significant challenges to DFT based computational methods.[46] It is unknown if a similar feature appears also for the suboxides. To minimize the sensitivity to this problem, we did not specifically focus on the pre-edge region in the analysis. We found out that the results presented in this work are not very sensitive to the energy range used.[47]

In order to gain more insight into the electronic structure at the interface region, we carried out calculations for the symmetry projected local density of unoccupied states[15] for each suboxide. These were obtained using the same framework that was employed for spectrum calculations. In terms of the Kohn-Sham orbitals $\phi_n(\mathbf{r})$ and their expression in spherical harmonic basis, $\phi_n(\mathbf{r}) = \sum_{l=0}^{l_{\max}} \sum_{m=-l}^{l} c_{lm}^n(r) Y_{lm}(\hat{\mathbf{r}})$, the local density of states is

$$\ell\mathrm{DOS}(E) = \sum_{n} \sum_{l=0}^{l_{\max}} \sum_{m=-l}^{l} \int_0^{R_{\max}} dr r^2 |c_{lm}^n(r)|^2 \delta(E - \omega_n), \quad (3)$$

where the sum over n includes the unoccupied electronic states. $R_{\max}$ determines the spatial region where the density

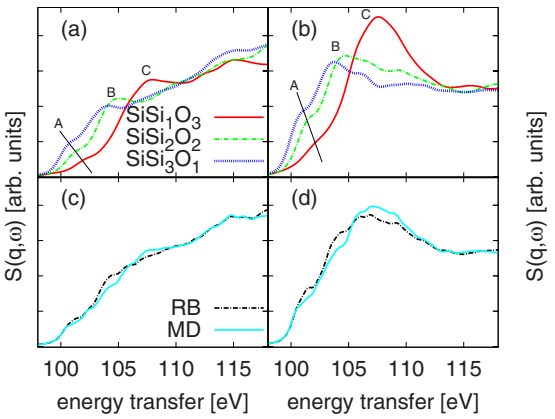

FIG. 3. (Color online) The upper figures show the calculated dynamic structure factors for the three different suboxides at (a) $q=2.3$ Å^{-1} and (b) $q=9.8$ Å^{-1}. The calculations for two different interface structural models (RB and MD, see the text) are shown in the lower figures with (c) $q=2.3$ Å^{-1} and (d) $q=9.8$ Å^{-1}.

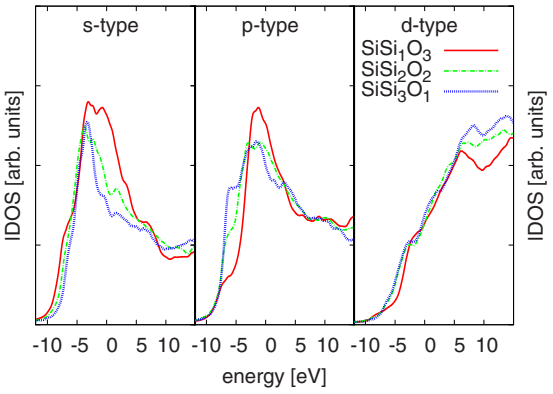

FIG. 4. (Color online) The symmetry decomposed local densities of unoccupied electronic states of the three suboxides. These were calculated using the framework presented in Ref. 31 and they demonstrate that the p-type ℓDOS is most sensitive to the oxidation state. The average energy of the highest occupied molecular orbital is −7.5 eV.

of states is analyzed and a typical choice is the radius of the Norman sphere of the excited site.[48] In practice its exact value only affects the absolute scale and the overall shape is almost independent of it. In this work we use the value 1.22 Å. The symmetry projected ℓDOS is found by including only the corresponding l terms of the sum.

III. RESULTS AND DISCUSSION

After carrying out the MD simulations and extracting the small clusters from the simulation snapshots, the calculations of XRS spectra were carried out for each cluster and those with the same oxidation state of the central Si site were averaged. For each suboxide, 40–50 model clusters were extracted. To mimick the lifetime broadening, the XRS spectra and ℓDOS curves were convoluted by Lorentzian line shape using the full width at half maximum (FWHM) of 0.2 eV. The spectra were also convoluted by Gaussian line shape to account for the experimental resolution, i.e., FWHM =0.6 eV for analyzing the results from series A and 1.4 eV for series B. The total calculated suboxide spectra are shown in Figs. 3(a) and 3(b) for two different momentum-transfer values (the directional averaging of $\mathbf{q}$ vectors was carried out). The chemical shift (features A) as a function of the oxidation state is evident and also other features (B and C) are clearly distinguishable. In particular, the position and intensity of the main peak (feature C) of $SiSi_1O_3$ is clearly different to $SiSi_2O_2$ and $SiSi_3O_1$ (features B).

The calculated total suboxide spectrum $S^{\mathrm{calc}}_{\mathrm{SiO}_x}(\mathbf{q},\omega)$ depends on the relative weights of the suboxides w_i,

$$S^{\mathrm{calc}}_{\mathrm{SiO}_x}(\mathbf{q},\omega)=\sum_{n=1}^{3} w_n S^{\mathrm{calc}}_{\mathrm{SiSi}_{4-n}\mathrm{O}_n}(\mathbf{q},\omega). \quad (4)$$

The weights w_i are predicted by the different structural models for suboxide contributions. We used two different models, namely, the random bonding (RB) model[49,50] and the MD model.[36] The RB model suggests a binomial distribution of the oxidation states, i.e., $w_1=w_3=0.29$, $w_2=0.43$. The MD simulation carried out in this work gives the second estimate for the proportions ($w_1=0.36$, $w_2=0.13$, and $w_3=0.51$). The higher amount of suboxides with the oxidation state +3 requires a smaller contribution of SiO_2 compared to Si to fulfill the sample's overall 1:1 stoichiometry. This model predicts a reduced weight of Si 2+ component and an increased weight of Si 3+ component which gives a more realistic description of the suboxide interfaces than the RB model, as suggested by several experiments.[51,52] The calculated spectra are shown in Figs. 3(c) and 3(d) which illustrates that the MD and RB models give very similar spectra. Therefore the overall contribution of the suboxides to the SiO XRS spectra can be described using either model.

The origin of the spectral features can be traced back to the local electronic structure in the vicinity of the silicon sites, which is described by the local density of unoccupied states. The ℓDOS curves (calculated in the presence of the half core hole) for the three suboxides are presented in Fig. 4 which show that the p-type ℓDOS is most sensitive to the oxidation state. This is related to the oxygen-silicon bonding that involves O $2p$ and Si $3p$ states. The measurement of the p-type ℓDOS from the Si $L_{\mathrm{II,III}}$ edge requires dipole forbidden transitions which are enhanced at high-momentum transfers.

Because the calculated suboxide spectrum is practically independent of the chosen structural model (MD or RB), we can use either one of them to determine the total amount of the suboxides, i.e., the value for a in Eq. (1). It is determined for each sample by a fitting procedure of the calculated and experimental suboxide spectra, i.e., by minimizing the integral

$$I(\mathbf{q})=\int_{100\ \mathrm{eV}}^{120\ \mathrm{eV}} d\omega |S_{\mathrm{exp}}(\mathbf{q},\omega)-[(1-a)\times S_{\mathrm{Si+SiO_2}}(\mathbf{q},\omega)+aS^{\mathrm{calc}}_{\mathrm{SiO}_x}(\mathbf{q},\omega)]|^2. \quad (5)$$

The reference spectrum $S_{\mathrm{Si+SiO_2}}(\mathbf{q},\omega)$ is approximated for series A by the spectrum of the sample annealed at T_a

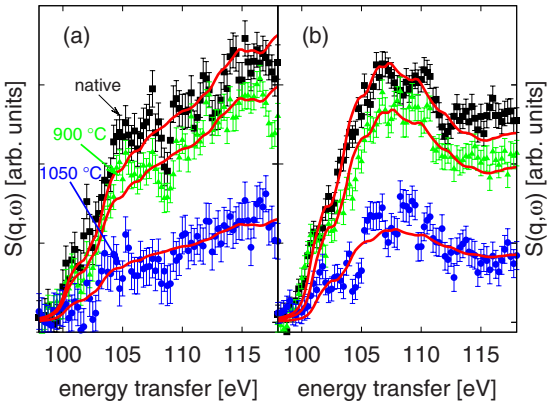

FIG. 5. (Color online) The extracted suboxide contributions to the total XRS spectra at (a) $q=2.4$ Å^{-1} and (b) $q=9.85$ Å^{-1}, using the amount of suboxides obtained by the fitting procedure described in the text and presented in Fig. 6. The solid curves show the calculated suboxide spectra. The scaling is the same for all curves and thus the intensity changes serve as a proof of the quality of the fitting procedure.

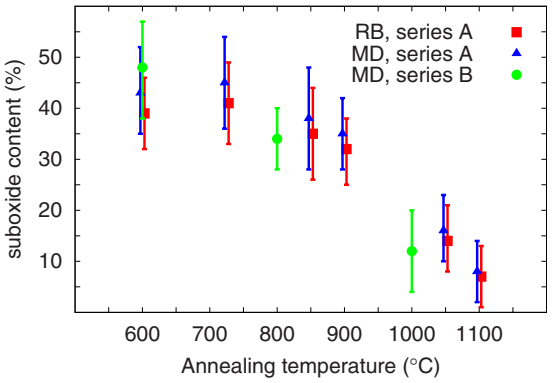

FIG. 6. (Color online) The suboxide content as a function of the annealing temperature shows that the amount of suboxides changes significantly at around 900 °C.

=1200 °C which is found to describe almost disproportionated SiO.[23] We use both low and high q spectra in the analysis so that the fitting procedure minimizes

$$I(q=2.4\ \text{Å}^{-1})+I(q=9.85\ \text{Å}^{-1}), \tag{6}$$

where the directional average of the **q** vectors is implied. In addition to the amount of suboxides, the integral was minimized also with respect to rigid energy shifts of 0–1 eV for the calculated spectrum. The resulting suboxide spectrum for three samples is shown in Fig. 5, illustrating a good agreement of the experimentally extracted and the calculated spectra. Almost all features in the experimental spectrum are reproduced by the calculation. A detailed analysis of these features would be valuable for the understanding of the physical properties of the material but it is out of the scope of this work. Here it is more important to note that the overall spectral shape of the total suboxide contribution differs significantly from that of Si and SiO_2, which improves the sensitivity of the fit to the suboxide content.

Figure 6 shows the obtained T_a-dependent suboxide content and demonstrates that the most significant structural changes take place at annealing temperatures above 900 °C where also the Si nanocrystal formation starts.[23] The error analysis of the suboxide content is not straightforward because numerous factors affect the quality of the fit. Compared to the accuracy of the calculations, the statistical error of the experimental spectra has only a minor effect. Thus a better estimate is obtained from the deviation of the low- and high-momentum-transfer results. This way we found out that the error can be estimated by requiring that the value of the integral [Eq. (6)] must not differ from its minimum value by more than 25%. As can be seen in Fig. 6, the estimated error bars quite well reflect the variation in the experimental data points.

Due to the fact that the shape of the total suboxide spectrum is similar either using MD or RB model, we fitted the spectra of series A using the XRS spectrum of the MD model, although the 1:1 stoichiometry is not fully conserved. The results are also presented in Fig. 6 and show no significant deviation from the RB model. We also carried out the analysis taking the different stoichiometry of MD model into account, which is possible for the sample series B where also Si and SiO_2 reference XRS spectra were measured. Thus the total spectrum of series B can be approximated by a superposition of weighted XRS spectra of Si and SiO_2 together with the calculated suboxide contribution from the MD model. Then the integral whose value is minimized can be written as

$$\int_{100\ \text{eV}}^{120\ \text{eV}} d\omega |S_{\text{exp}}(\mathbf{q},\omega) - [aS^{\text{calc}}_{\text{SiO}_x}(\mathbf{q},\omega) + b \times S_{\text{Si}}(\mathbf{q},\omega) + cS_{\text{SiO}_2}(\mathbf{q},\omega)]|^2, \tag{7}$$

where a, b, and c have to obey the stoichiometry condition $(2.15a+4c=2)$ and sum up to 1.0. The resulting suboxide content is shown in Fig. 6 for three samples and the result agrees well with those extracted from the spectra of series A.

The proportion of suboxides in the native sample (40%) is found to be relatively high compared to estimates given in earlier studies.[4] Using the current approach to determine the suboxide content of course relies strongly on underlying model calculations. The suboxide content might be slightly overestimated due to the fact that spectral features from Si, Si 1+, and Si 2+ components are not well separated. It has to be noted that independently from the model we use to extract the suboxide content in the samples, an estimate of the lower limit of the suboxide contribution can be given. This is obtained by requiring that the suboxide spectrum cannot be negative. Using this method we yield a lower limit of $20\pm3\%$ for the native sample and those annealed below 900 °C. Moreover, the relative change in suboxide content is in line with the phase-separation process.[23]

The origin of the T_a dependency of the XRS spectrum is suggested to be the decreasing suboxide content that is accompanied with the growth of the Si and SiO_2 regions. Another possibility is that the changes in the spectral shape are due to the crystallization of amorphous silicon nanoclusters, which takes place at this temperature range.[6,23] We excluded

this option by comparing our measured low-momentum-transfer near-edge spectra with previously published[53] EELS data of amorphous and crystalline silicons. The crystallization causes most significant changes in the EELS spectra in the pre-edge region (100 eV) while the 102–106 eV region is very similar for both phases. The decreasing suboxide content is therefore the only plausible explanation to the observed differences in the spectra. This is in accordance with the situation of amorphous GeO that also disproportionates into regions of nanocrystalline Ge and amorphous GeO_2 but where the crystallization takes place at a different annealing temperature range.[54,55]

IV. CONCLUSIONS

We have used experimental and computational methods to investigate the microscopic structure of the internal suboxide interfaces in disproportionating a-SiO. The sensitivity of the near-edge XRS spectrum to the local atomic structure in the vicinity of the Si atoms allows a detailed analysis of the interface contribution. The presence of suboxides in these regions is confirmed and the proposed framework demonstrates how the suboxide contribution to the Si $L_{\mathrm{II,III}}$ near-edge spectrum can be extracted and used for determining the amount of the suboxides. Our results suggest a significant contribution of suboxides in the native material of about 40% which decreases during annealing. When nanocrystal formation starts [between 900 and 1000 °C (Ref. 23)] the suboxide contribution is approximately 10%. We also presented symmetry decomposed local densities of unoccupied states for the three suboxides which shows strong sensitivity of p-type ℓDOS to the oxidation state. This favors measurements at high q if one would like to distinguish different suboxides.

Our framework can be further generalized to gain an even more accurate picture of the suboxide interfaces. In principle, the presented fitting procedure can determine the amount of different suboxides directly. This will require experiments with better energy resolution and statistics, as well as more accurate calculations including excitonic effects, spin-orbit coupling, and the crystallization of the Si nanoclusters.

ACKNOWLEDGMENTS

The authors acknowledge Advanced Photon Source for the synchrotron radiation and thank T. T. Fister, M. Balasubramanian, and R. Gordon for assistance in using beamline XOR/PNC 20-ID. We also thank J. A. Soininen for useful discussions. This work has been supported by the Academy of Finland (Contracts No. 1110571 and No. 1127462), the National Graduate School in Materials Physics, DAAD (Grants No. 1127504 and No. 313-PPP-SF/08-IK), and DFG (Grant No. TO 169/14-1).

*arto.sakko@helsinki.fi

[1] A. Zimina, S. Eisebitt, W. Eberhardt, J. Heitmann, and M. Zacharias, Appl. Phys. Lett. **88**, 163103 (2006).
[2] V. Kapaklis, C. Politis, P. Poulopoulos, and P. Schweiss, Appl. Phys. Lett. **87**, 123114 (2005).
[3] M. Mamiya, H. Takei, M. Kikuchi, and C. Uyeda, J. Cryst. Growth **229**, 457 (2001).
[4] A. Hohl, T. Wieder, P. A. van Aken, T. E. Weirich, G. Denninger, M. Vidal, S. Oswald, C. Deneke, J. Mayer, and H. Fuess, J. Non-Cryst. Solids **320**, 255 (2003).
[5] J. Heitmann, F. Müller, L. Yi, M. Zacharias, D. Kovalev, and F. Eichhorn, Phys. Rev. B **69**, 195309 (2004).
[6] S. Boninelli, F. Iacona, G. Franzó, C. Bongiorno, C. Spinella, and F. Priolo, J. Phys.: Condens. Matter **19**, 225003 (2007).
[7] O. Jambois, H. Rinnert, X. Devaux, and M. Vergnat, J. Appl. Phys. **100**, 123504 (2006).
[8] G. Ledoux, J. Gong, F. Huisken, O. Guillois, and C. Reynaud, Appl. Phys. Lett. **80**, 4834 (2002).
[9] M. Luppi and S. Ossicini, Phys. Rev. B **71**, 035340 (2005).
[10] D. König, J. Rudd, M. A. Green, and G. Conibeer, Phys. Rev. B **78**, 035339 (2008).
[11] C. Sternemann, J. A. Soininen, M. Volmer, A. Hohl, G. Vanko, S. Streit, and M. Tolan, J. Phys. Chem. Solids **66**, 2277 (2005).
[12] J. J. van Hapert, A. M. Vredenberg, E. E. van Faassen, N. Tomozeiu, W. M. Arnoldbik, and F. H. P. M. Habraken, Phys. Rev. B **69**, 245202 (2004).
[13] J. Stöhr, *NEXAFS Spectroscopy* (Springer-Verlag, Berlin, 1992).
[14] W. Schülke, *Electron Dynamics by Inelastic X-Ray Scattering* (Oxford University Press, Oxford, 2007).
[15] J. A. Soininen, A. Mattila, J. J. Rehr, S. Galambosi, and K. Hämäläinen, J. Phys.: Condens. Matter **18**, 7327 (2006).
[16] U. Bergmann, P. Glatzel, and S. P. Cramer, Microchem. J. **71**, 221 (2002).
[17] H. Conrad, F. Lehmkühler, C. Sternemann, A. Sakko, D. Paschek, L. Simonelli, S. Huotari, O. Feroughi, M. Tolan, and K. Hämäläinen, Phys. Rev. Lett. **103**, 218301 (2009).
[18] J. S. Tse, D. M. Shaw, D. D. Klug, S. Patchkovskii, G. Vankó, G. Monaco, and M. Krisch, Phys. Rev. Lett. **100**, 095502 (2008).
[19] M. Balasubramanian, C. S. Johnson, J. O. Cross, G. T. Seidler, T. T. Fister, E. A. Stern, C. Hamner, and S. O. Mariager, Appl. Phys. Lett. **91**, 031904 (2007).
[20] K. Hämäläinen, S. Galambosi, J. A. Soininen, E. L. Shirley, J.-P. Rueff, and A. Shukla, Phys. Rev. B **65**, 155111 (2002).
[21] W. L. Mao, H. K. Mao, Y. Meng, P. J. Eng, M. Y. Hu, P. Chow, Y. Q. Cai, J. F. Shu, and R. J. Hemley, Science **314**, 636 (2006).
[22] T. Pylkkänen, V. M. Giordano, J.-C. Chervin, A. Sakko, M. Hakala, J. A. Soininen, K. Hämäläinen, G. Monaco, and S. Huotari, J. Phys. Chem. B **114**, 3804 (2010).
[23] O. M. Feroughi, C. Sternemann, Ch. J. Sahle, M. A. Schroer, H. Sternemann, H. Conrad, A. Hohl, G. T. Seidler, J. Bradley, T. T. Fister, M. Balasubramanian, A. Sakko, K. Pirkkalainen, K. Hämäläinen, and M. Tolan, Appl. Phys. Lett. **96**, 081912 (2010).
[24] T. T. Fister, G. T. Seidler, L. Wharton, A. R. Battle, T. B. Ellis, J. O. Cross, A. T. Macrander, W. T. Elam, T. A. Tyson, and Q. Quian, Rev. Sci. Instrum. **77**, 063901 (2006).

[25] H. Sternemann, C. Sternemann, G. T. Seidler, T. T. Fister, A. Sakko, and M. Tolan, J. Synchrotron Radiat. **15**, 162 (2008).
[26] $\int_{100\ \mathrm{eV}}^{120\ \mathrm{eV}} d\omega S_{\mathrm{SiO}_x}(\mathbf{q},\omega) = \int_{100\ \mathrm{eV}}^{120\ \mathrm{eV}} d\omega S_{\mathrm{Si+SiO}_2}(\mathbf{q},\omega)$
[27] J. A. Soininen and E. L. Shirley, Phys. Rev. B **64**, 165112 (2001).
[28] E. L. Shirley, Phys. Rev. Lett. **80**, 794 (1998).
[29] J. A. Soininen, K. Hämäläinen, W. A. Caliebe, C.-C. Kao, and E. L. Shirley, J. Phys.: Condens. Matter **13**, 8039 (2001).
[30] J. A. Soininen, A. L. Ankudinov, and J. J. Rehr, Phys. Rev. B **72**, 045136 (2005).
[31] A. Sakko, M. Hakala, J. A. Soininen, and K. Hämäläinen, Phys. Rev. B **76**, 205115 (2007).
[32] C. Ceriani, A. Laio, E. Fois, A. Gamba, R. Martoňák, and M. Parrinello, Phys. Rev. B **70**, 113403 (2004).
[33] M. Woodley and R. Catlow, Nature Mater. **7**, 937 (2008).
[34] T. Watanabe, D. Yamasaki, K. K. Tatsumura, and I. Ohdomari, Appl. Surf. Sci. **234**, 207 (2004).
[35] J. Samela, K. Nordlund, V. N. Popok, and E. E. B. Campbell, Phys. Rev. B **77**, 075309 (2008).
[36] F. Djurabekova and K. Nordlund, Phys. Rev. B **77**, 115325 (2008).
[37] This choice of cutoff gave very similar results to using 4.5 Å.
[38] L. Triguero, L. G. M. Pettersson, and H. Ågren, Phys. Rev. B **58**, 8097 (1998).
[39] STOBE-DEMON version 3.0 (2009), K. Hermann, L. G. M. Pettersson, M. E. Casida, C. Daul, A. Goursot, A. Koester, E. Proynov, A. St-Amant, and D. R. Salahub. Contributing authors: V. Carravetta, H. Duarte, C. Friedrich, N. Godbout, J. Guan, C. Jamorski, M. Leboeuf, M. Leetmaa, M. Nyberg, S. Patchkovskii, L. Pedocchi, F. Sim, L. Triguero, and A. Vela.
[40] J. C. Slater, Adv. Quantum Chem. **6**, 1 (1972).
[41] B. Hammer, L. B. Hansen, and J. K. Nørskov, Phys. Rev. B **59**, 7413 (1999).
[42] J. P. Perdew, K. Burke, and M. Ernzerhof, Phys. Rev. Lett. **77**, 3865 (1996).
[43] S. Huzinaga, L. Seijo, Z. Barandiarán, and M. Klobukowski, J. Chem. Phys. **86**, 2132 (1987).
[44] L. G. M. Pettersson, U. Wahlgren, and O. Gropen, J. Chem. Phys. **86**, 2176 (1987).
[45] C. Sternemann, J. A. Soininen, S. Huotari, G. Vankó, M. Volmer, R. A. Secco, J. S. Tse, and M. Tolan, Phys. Rev. B **72**, 035104 (2005).
[46] S. Albrecht, L. Reining, R. Del Sole, and G. Onida, Phys. Rev. Lett. **80**, 4510 (1998).
[47] The effect of using, e.g., energy range 105–115 eV (instead of 100–120 eV) in the fitting procedure, described in Sec. III, is much smaller than the error bars in Fig. 6.
[48] M. P. Prange, J. J. Rehr, G. Rivas, J. J. Kas, and John W. Lawson, Phys. Rev. B **80**, 155110 (2009).
[49] H. R. Philipp, J. Phys. Chem. Solids **32**, 1935 (1971).
[50] H. R. Philipp, J. Non-Cryst. Solids **8-10**, 627 (1972).
[51] F. G. Bell and L. Ley, Phys. Rev. B **37**, 8383 (1988).
[52] J. H. Oh, H. W. Yeom, Y. Hagimoto, K. Ono, M. Oshima, N. Hirashita, M. Nywa, A. Toriumi, and A. Kakizaki, Phys. Rev. B **63**, 205310 (2001).
[53] C. Tarrio and S. E. Schnatterly, J. Opt. Soc. Am. B **10**, 952 (1993).
[54] A. Schacht, C. Sternemann, A. Hohl, H. Sternemann, Ch. J. Sahle, M. Paulus, and M. Tolan, J. Non-Cryst. Solids **355**, 1285 (2009).
[55] Ch. J. Sahle, C. Sternemann, H. Conrad, A. Herdt, O. M. Feroughi, M. Tolan, A. Hohl, R. Wagner, D. Lützenkirchen-Hecht, R. Frahm, A. Sakko, and K. Hämäläinen, Appl. Phys. Lett. **95**, 021910 (2009).